ELSEVIER

Earth and Planetary Science Letters 193 (2001) 129–142

EPSL

www.elsevier.com/locate/epsl

The petrophysical properties of deformation bands in relation to their microstructure

Steven R. Ogilvie *, Paul W.J. Glover

Department of Geology and Petroleum Geology, University of Aberdeen, Aberdeen AB24 3UE, Scotland, UK

Received 15 January 2001; received in revised form 2 July 2001; accepted 30 August 2001

Abstract

Deformation bands are significant discontinuities in reservoir sandstones providing baffles to the migration of fluids and acting as seals for hydrocarbon accumulations. Their contribution to these processes is dependent upon a range of inter-related factors including lateral continuity, relative displacement, reservoir geohistories and rock microstructure. Deformation bands have millimetre-scale displacements, which are smaller than the seismic resolution, and hence the study of their microstructure from reservoir cores is a necessary tool in the prediction of their fault seal potential. The latter is only achieved if detailed petrophysical measurements of fault microstructure are carried out using techniques, which are suitable for measurement of very low permeability fault rock at the relevant scale. Conventional techniques of fault rock porosity and permeability determination invite host rock bias in measurement and inevitably underestimate the potential of these structures as fluid barriers. Pressure decay probe permeametry used in this study has the advantage of measuring small volumes of rock at finer spatial resolutions and detailed permeability distributions around common types of deformation bands are obtained. Together with supporting data provided by conventional core analysis techniques, these measurements show that the greatest differences in petrophysical properties relative to host rock occur in those bands, which have experienced cataclasis. These results provide valuable input into reservoir simulation models and help reduce much of the uncertainty regarding the role of different types of deformation bands in fault seal.

Keywords: planar deformation features; ultrastructure; high-resolution methods; physical properties; reservoir rocks

1. Introduction

The microstructure of fault rocks has recently formed the basis of numerous studies aimed at a better understanding and prediction of fault seal processes [1–6]. The latter is only possible by detailed understanding of the processes, which control the evolution of fault rocks and quantification of the petrophysical properties of the different fault rocks present in the hydrocarbon field [7]. There is, however, a dearth of published petrophysical data on deformation bands in the literature. The majority of work has focused upon 'closed' faults with deformed fabrics relative to the host rock. These structures often have dramatic reductions in porosity and permeability,

* Corresponding author. Tel.: +44-1224-273456; Fax: +44-1224-272785.
E-mail address: s.ogilvie@abdn.ac.uk (S.R. Ogilvie).

0012-821X/01/$ – see front matter
PII: S0012-821X(01)00492-7

rendering them non-conductive to fluid flow. Commonly referred to as deformation bands [3,4,8–10], they have throws in the order of a few millimetres and hence are below the resolution of seismic data. It is therefore important to characterise their internal microstructure from core recovered from drilling programmes for effective fault seal analysis.

Deformation bands which have formed by reductions in grain size and sorting aided by increased packing [10] are referred to as 'cataclastic' [11]. These are common in the best quality sandstone reservoirs (i.e. highest depositional porosities and permeabilities) and have markedly reduced porosity and permeability relative to their host rock [4,12,13]. The principal mechanism of porosity reduction is a wider grain size distribution that permits closer packing, associated with grain size reduction concomitant with increasing strain, confining pressure and fault displacement [14,15]. It is not always possible to predict displacement from the degree of grain comminution, as displacement may not be accommodated by grain fracturing during the late stages of deformation band formation [10]. This is a result of the 'cushioning effect' that smaller grains have upon larger grains, offering a more even pressure than that if a few large grains surround a central grain, and therefore preventing grain fracture. The 'nearest neighbour theory' of Sammis et al. [15] is however in operation in host rock pods (lenses of undeformed sandstone sandwiched in between deformation band zones) where microfractures are a result of stress concentrations at point contacts between similar sized grains [10]. Cataclastic deformation bands form sequentially by strain hardening from single bands with millimetre-scale displacement to compound zones of deformation bands [8,9]. Compound zones may develop slip surfaces across which there is metre-scale slip.

Deformation by clay smearing [16,17] and by the mixing of phyllosilicate (clay) material [5,18,19] into deformation bands has also been addressed. It has recently been suggested that as little as 20% phyllosilicate content of a deformation band is sufficient to give it a comparable fault sealing potential to clay smears [5]. This observation removes the simple assumption that fault seal is only accomplished through clay smearing and by the juxtaposition of permeable and impermeable sandstones. Cemented deformation bands [20] are common reservoir seals and negate the applicability of simple seal prediction based only on host rock lithology [7]. These cements are a result of precipitation from fluids flushing along the fault zone, or in cataclasites they may result from attraction of dissolved species to the high concentration of nucleation sites on newly created fracture surfaces [7]. Healing quartz cement is common within fractured grains in deformation bands. High temperatures and the presence of reactive pore fluids speed the healing process and reduce the time required for crack closure in quartz [21]. This implies that open microfractures are young and have remained at relatively low temperatures [22] or that there has been an absence of pore fluids loaded with dissolved minerals.

Whilst appreciating the need for integrated geometrical and microstructural studies of fault rocks for effective fault seal analysis [4,23], this paper focuses upon the internal structure of a variety of deformation bands from different settings in relation to their petrophysical properties. These discontinuities influence the production history of most reservoirs, and their impact upon fault damage zones in high porosity sandstones has been extensively studied using relatively low-resolution techniques such as conventional core analysis and outcrop minipermeametry [4,5]. Many deformation bands, however, have permeabilities considerably lower than 10^{-17} m^2 (0.01 mD), the conventional resolution of traditional Hassler sleeve gas permeametry.

In this study, a database of deformation band petrophysical properties has been generated. Such data are necessary to support a developing understanding of (i) the relationship between the microstructure and petrophysical properties of deformation bands, (ii) their influence upon fluid flow, and (iii) their role in fault seal analysis [6]. Such data enable more accurate fault seal predictions to be made, which is highly important considering that exploration efforts are being increasingly aimed at more complex and/or fractured reservoirs.

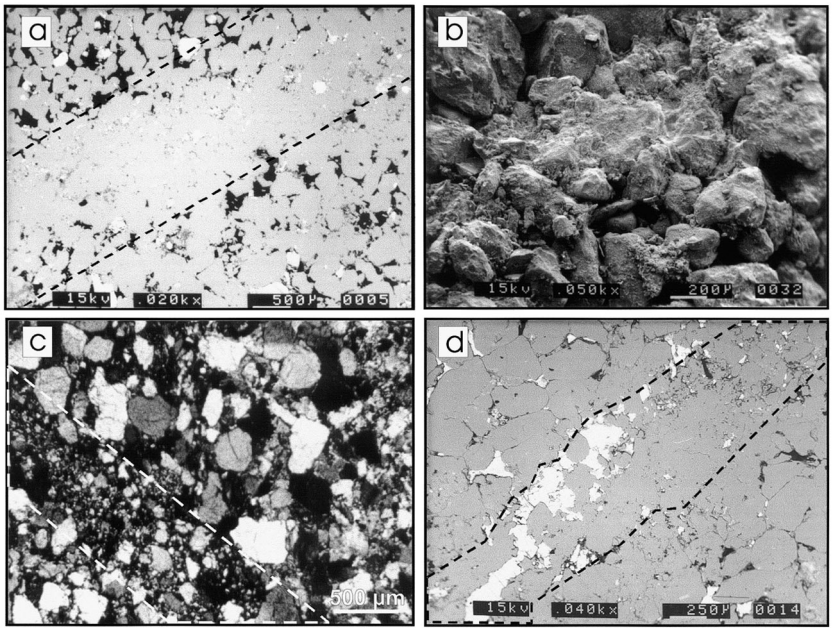

Fig. 1. The variable microstructures of deformation bands in reservoir sandstones. (a) SEM, backscattered electron image showing cataclastic deformation bands hosted by high porosity, clean sandstone (porosity in black). This region of the sandstone has experienced significant reductions in grain size despite containing host rock size grains. (b) SEM, secondary electron image of the deformation band in (a) illustrating the highly crushed nature of the deformation band fabric relative to the host. (c) Clay-rich deformation band from southern North Sea hosted by texturally and mineralogically immature sandstone. (d) Cataclastic deformation band cemented by anhydrite from texturally immature southern North Sea sandstones.

2. Petrography of deformation bands

Deformation bands have displacements in the order of 1 mm to 2 cm, are tectonic in origin, and tend to cluster around larger, seismically resolvable master faults [1,4,23,24]. The deformation bands are laterally continuous in outcrop and at well-scale, tending to distribute the displacement over a significant volume of rock compared to the volume of the original deformation band before splitting into two or more bands. Synsedimentary and compactional sub-seismic faults [18,25] have a more random spatial distribution relative to master faults. These are not commonly reported in the literature, and are not considered in this study.

The deformation bands are recognised in thin section as linear distributions of partially to completely deformed grains with associated porosity reductions but rarely containing a clearly defined slip surface (Fig. 1). Examples of cataclastic deformation bands are shown in Fig. 1a,b where significant reductions in macro-porosity and permeability are a function of grain size reduction, and correlate well with reductions in sorting [26]. The latter is a result of the occurrence of undeformed host-sized grains in a groundmass of comminuted quartz, feldspar and rock fragments. The presence of these larger, rounded grains suggests that during initial straining, the quartz grains were disaggregated and incorporated into the matrix by grain boundary fracture mechanisms [27] and abraded during rotation in the deformation band matrix [12]. Host-sized grains also occur in a clay matrix in the clay-rich deformation bands (Fig. 1c). These structures have experienced varying amounts of grain comminution and cementation (quartz, anhydrite, calcite, etc.). They also have a more homogeneous distribution of clays (often authigenic illite) compared to the host rock, which have been mixed into the bands during the deformation process, with very similar

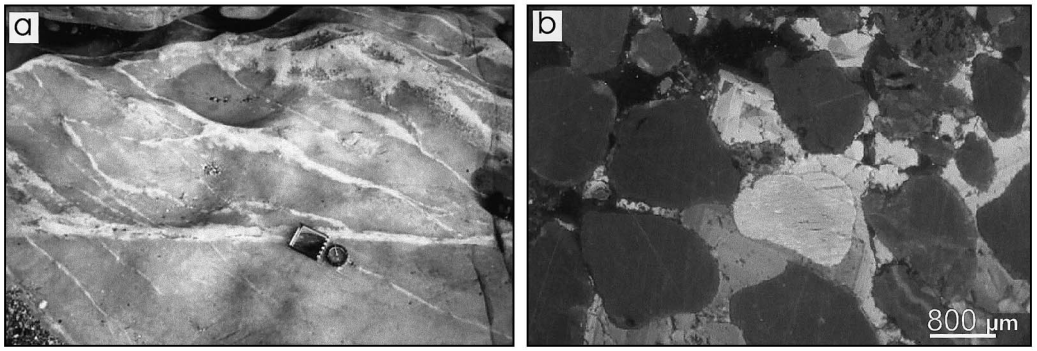

Fig. 2. Dilational deformation bands cemented by fluorite. (a) Compartmentalisation of the Hopeman Sandstone, NE Scotland by fluorite cemented deformation bands. The fluorite cements a narrow zone on either side of individual fault strands. (b) Cathodoluminescence image showing chemical zoning within the fluorite cements indicating rapidly evolving fluid flow. Here, no grain size reduction or compaction is observed as dilation has been the dominant process.

grain size distributions to the host rock (Fig. 1c). In fact, clay-rich deformation bands in sandstones have similar sealing potential to clay smears, which characterise shaley lithologies [5].

The contribution of these structures to fault sealing is invariably depth related. For example, the mechanical reduction of porosity and permeability along fault planes is more likely with increasing confining pressure. The precipitation of cements is also more likely at greater depths. In Fig. 1d anhydrite cement is concentrated in the crushed pores of a cataclastic deformation band, suggesting that this structure has been reactivated to provide a pathway for fluid flow. Similar deformation bands have been reported in reservoirs from the UK sector of the southern North Sea [6,28]. The deformation band represents advanced levels of cataclasis giving a better-sorted grain size distribution (minus cement) than the host rock. It is probable that cement nucleation is easier in the smaller pores as it requires less free energy than if it were to precipitate in larger, host rock pores [7]. Such a mechanism indicates that enhanced fluid movement may occur along the deforming zone during faulting. It is therefore unlikely that seismic pumping [29] is the mechanism for fluid migration. Seismic valving may be involved, in which fluid overpressure within a reservoir juxtaposed against the deformation band drives fluid movement [30]. Fluorite cementation in relation to dilational deformation bands in the Permian Hopeman Sandstone, NE Scotland is illustrated in Fig. 2. The cement is restricted to a narrow, pervasive region around the band lending credence to a suction pump theory of cement derivation (Fig. 2a) [31,32].

3. Petrophysical techniques

A database of petrophysical properties of deformation bands from the southern North Sea and from outcrop sandstones in the UK has been produced, which incorporates critical properties, requiring quantification for successful fault seal analysis. These are (i) porosity, (ii) permeability, (iii) capillary entry pressures, (iv) irreducible water saturation, S_{WI}, (v) grain size distributions and (vi) pore throat diameter distributions.

These properties have been obtained from a range of conventional core analyses including (i) mercury injection capillary pressure (MICP) analysis, (ii) helium porosimetry, (iii) thin-section image analysis, (iv) scanning electron microscopy (SEM), and (v) Hassler sleeve gas permeametry (HSGP). Permeability has also been obtained using the novel pressure decay probe permeametry (PDPK) technique.

The MICP technique has been used to measure capillary entry pressures and to calculate porosity, pore radii and irreducible water saturations. Capillary entry pressure, P_c, can be used to determine the sealing properties of a deformation band [4]. This is the minimum pressure required for a

non-wetting phase (e.g. hydrocarbons) to displace the connate water out of the pore space:

$$P_c = \frac{2\gamma\cos\theta}{R}$$

where R is the effective interconnected pore throat radius, γ is interfacial tension and θ is the wetting angle.

Capillary pressure curves were generated for host rock and deformation band samples. The MICP technique has the advantage over core plug porosimetry in that the deformation bands can be separated from their host rock, hence the data are specific to the deformation band or host rock respectively. Helium porosimetry does, however, reach smaller pores than mercury porosimetry, and therefore is used to provide mean (effective) porosity values. Image analysis of thin sections impregnated with blue epoxy was also used to measure the porosity variation within and around the deformation band zones. Changes of porosity *in tandem* with textural and mineralogical changes were also observed using a scanning electron microscope (SEM). Grain diameter distributions of deformation bands and their associated host rock were calculated from a series of SEM photographs taken across deformation bands.

The permeability of core plugs was measured using HSGP and corrected for the klinkenberg effect. This corrects for slippage of gas along the rock walls at low pressures (low densities). The deformation bands account for about 30% of the plugs, hence there is a host rock bias in measurement. A pressure decay probe permeameter [26,33] was used therefore to provide a more detailed permeability distribution of deformation band zones of representative samples of deformation bands. Depending upon grid spacing, the micro-permeability of individual structures can be accurately measured by this method without separating them from their host rock. This technique measures the permeability of the rock by the release of a pulse of nitrogen gas through a laser-guided probe into the rock surface at 1 mm diameter nodes on a pre-defined pencilled grid drawn on the rock surface. Pilot tests have revealed that graphite from the pencilling does not clog the pores of the rock, and has no influence upon permeability. The pressure decay of nitrogen gas was monitored and used to calculate the slip-corrected permeability at a given node on the grid. The permeabilities were obtained using a modified Darcy's equation [33]. These were grouped into 12 bins and plotted as two-dimensional (2D) permeability contour maps [26]. This technique is particularly advantageous in the measurement of low fault rock permeabilities as it (i) has a higher spatial resolution than HSGP in measuring smaller volumes of rock, (ii) can measure permeabilities as low as 10^{-18} m^2 (0.001 mD) (cf. conventional limit of 10^{-17} m^2 (0.01 mD) for HSGP), and (iii) high-resolution (< 5 mm) permeability profiles of rock surfaces can be produced.

4. Results: petrophysical properties

The petrophysical properties for the deformation band samples and their host rock are given in Table 1. A combination of 2D and 3D measurements allows accurate petrophysical characterisation of common types of deformation bands.

4.1. Porosity

3D porosities of 1 inch core plugs were measured using helium porosimetry and the offcuts subjected to mercury injection capillary pressure (MICP) analysis and to thin-section image analysis. Porosities are dependent upon the scale of measurement, but significant reductions are recorded using all techniques. The most significant differences in MICP porosities between sample pairs are for the cataclastic and dilational cemented deformation bands relative to the host, where up to 50 and 75% reductions respectively are observed (Table 1; Fig. 1a,b). By contrast, the reduction in porosity in clay-rich and cataclastic cemented deformation bands relative to host sandstone is no greater than 25% (Table 1; Fig. 1c,d). Helium technique porosities from core plugs show less contrast between host rock and deformation band samples. This is because these are mean values of deformation band and attached host rock. There are greater differences

Table 1
Petrophysical data for cemented and uncemented deformation bands

	S_{WI} (%)	He porosity (%)	Capillary entry pressure, P_c (Pa)	Hg porosity (%)	Image analysis porosity (%)	HSGP, K_L (m^2)		PDPK, K_L (m^2)	Pore throat radii, R (μm)
						Hz	Vt		
Cataclastic deformation bands (Permian Hopeman Sandstone, NE Scotland; southern North Sea sandstones)									
H1	32.8	15.5	1.3×10^{6}	15.3	30.0	6.6×10^{-15}	–	1.8×10^{-15}	0.49
D1	66.5	10.8	1.7×10^{6}	8.13	15.0	4.0×10^{-16}	2.3×10^{-15}	1.1×10^{-15}	3.07
H2	0.00	25.5	1.7×10^{5}	21.2	16.5	1.3×10^{-12}	–	3.9×10^{-13}	16.6
D2	67.9	9.50	2.3×10^{6}	7.23	8.20	4.5×10^{-14}	8.5×10^{-16}	2.9×10^{-18}	11.6
H3	11.3	25.0	1.5×10^{5}	19.6	22.2	1.7×10^{-12}	7.1×10^{-13}	1.3×10^{-12}	0.69
D3	62.9	13.2	1.7×10^{6}	9.01	2.86	5.5×10^{-13}	6.7×10^{-15}	1.5×10^{-14}	1.44
H4	31.0	16.5	1.6×10^{5}	14.4	33.0	2.8×10^{-14}	–	3.2×10^{-13}	13.5
D4	52.1	2.50	1.9×10^{6}	11.2	0.40	4.7×10^{-16}	1.4×10^{-16}	5.9×10^{-17}	13.3
Cemented cataclastic deformation bands (southern North Sea sandstones)									
H5	73.9	8.93	1.9×10^{6}	7.50	12.3	1.7×10^{-16}	8.8×10^{-17}	3.9×10^{-16}	0.48
D5	76.9	5.60	3.6×10^{6}	6.60	10.0	1.9×10^{-16}	1.9×10^{-16}	2.9×10^{-16}	0.49
H6	84.0	5.04	1.2×10^{7}	4.39	10.2	8.8×10^{-17}	8.8×10^{-17}	2.2×10^{-15}	0.63
D6	73.4	6.33	2.8×10^{6}	6.69	4.50	1.9×10^{-16}	4.9×10^{-17}	5.9×10^{-17}	0.38
Cemented (dilational) deformation bands (Permian Hopeman Sandstone, NE Scotland)									
H7	0	34.7	1.6×10^{5}	20.4	26.0[a]	3.3×10^{-15}	–	7.4×10^{-13}	18.7
D7	87.9	5.80	3.3×10^{6}	3.41	24.5[a]	3.4×10^{-16}	9.9×10^{-18}	9.9×10^{-18}	19.2
H8	50.3	23.2	1.2×10^{5}	11.0	31.3[a]	1.2×10^{-12}	–	8.9×10^{-13}	22.9
D8	92.3	6.60	5.1×10^{6}	2.08	21.8[a]	6.0×10^{-15}	4.9×10^{-17}	2.9×10^{-14}	0.13
Clay-rich deformation bands (southern North Sea sandstones)									
H9	43.3	16.0	7.4×10^{5}	11.4	11.0	8.6×10^{-15}	3.3×10^{-15}	6.1×10^{-15}	2.48
D9	52.1	14.7	2.7×10^{6}	8.50	8.00	3.1×10^{-15}	3.9×10^{-16}	5.1×10^{-15}	0.93
H10	46.9	17.6	1.8×10^{6}	12.2	16.4	2.6×10^{-14}	–	1.4×10^{-14}	0.39
D10	62.8	16.2	1.8×10^{6}	9.56	13.2	1.3×10^{-14}	–	7.4×10^{-15}	5.82
H11	51.6	12.7	1.1×10^{6}	11.2	18.4	9.7×10^{-16}	7.8×10^{-16}	5.1×10^{-14}	0.98
D11	61.5	7.91	2.1×10^{6}	10.7	12.6	1.2×10^{-16}	2.8×10^{-16}	1.6×10^{-15}	2.48
H12	62.1	8.60	4.3×10^{6}	9.05	7.00	3.1×10^{-16}	1.9×10^{-15}	6.8×10^{-16}	0.79
D12	67.3	8.41	7.1×10^{6}	7.98	1.11	4.7×10^{-16}	4.6×10^{-15}	1.2×10^{-16}	0.61
H13	46.9	10.8	9.4×10^{5}	14.9	14.6	9.2×10^{-16}	–	1.6×10^{-15}	2.41
D13	62.7	10.6	8.1×10^{5}	11.1	5.90	9.1×10^{-16}	7.9×10^{-16}	7.8×10^{-16}	1.21

H, host rock; D, deformation band; S_{WI}, irreducible water saturation (%); K_L, klinkenberg-corrected permeability (m^2); HSGP, Hassler sleeve gas permeability (m^2); PDPK, pressure decay probe permeametry (m^2); Hz, horizontal plug with deformation band parallel to long axis; Vt, vertical plug with deformation band perpendicular to long axis.

[a] Skeletal porosities.

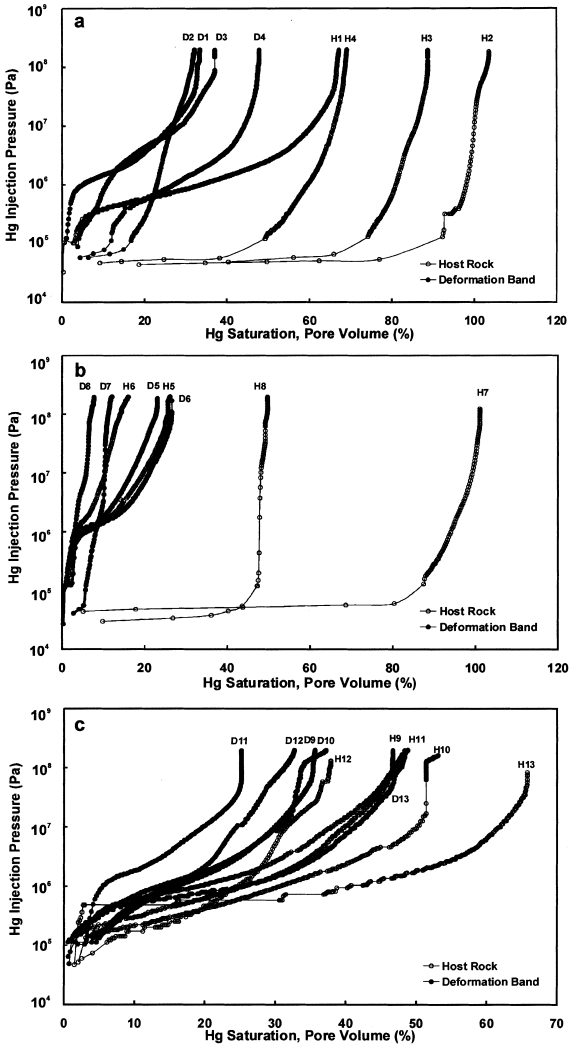

Fig. 3. Mercury injection capillary pressure curves for host rock and deformation bands listed in Table 1, (a) cataclastic, (b) cataclastic and dilational cemented and (c) clay-rich.

in image-analysed porosities particularly in the cataclastic deformation bands, but there are also significant changes in the clay-rich samples (Table 1).

4.2. Capillary pressures

Mercury injection-derived capillary pressure curves are presented in Fig. 3. There are considerable differences between the capillary pressure

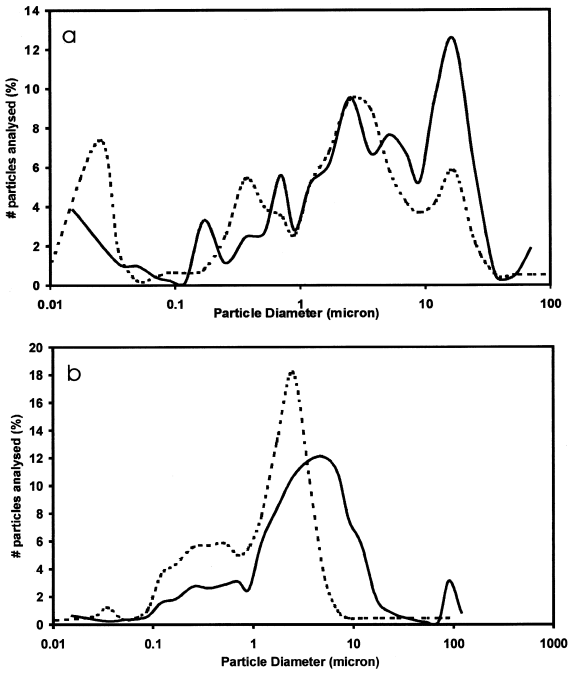

Fig. 4. Grain size distributions for representative clay-rich (a) and cataclastic (b) deformation bands (dashed line) and their host rocks (solid line). These have been measured from SEM photographs across deformation bands. The clay-rich deformation bands have similar grain size distributions to their host. The cataclastic deformation bands have approximately half the modal grain size of the host rock at a point perhaps representing the frictional strength of the rock.

curves of the host and deformation band samples, from which S_{WI} was calculated. The greatest differences in capillary pressures, P_c, are for the

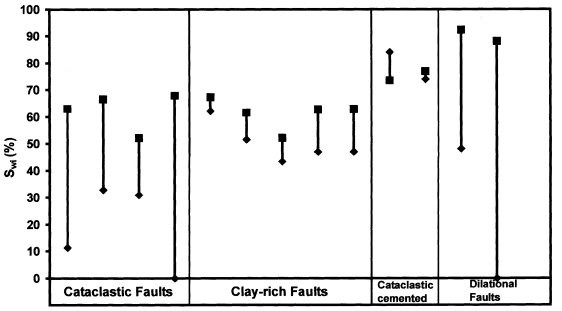

Fig. 5. Irreducible water saturation (S_{WI}) variation between deformation bands (square symbols) and host rock (diagonal symbols). The cataclastic deformation bands and dilational cemented deformation bands have the greatest differences in S_{WI} to their host rock.

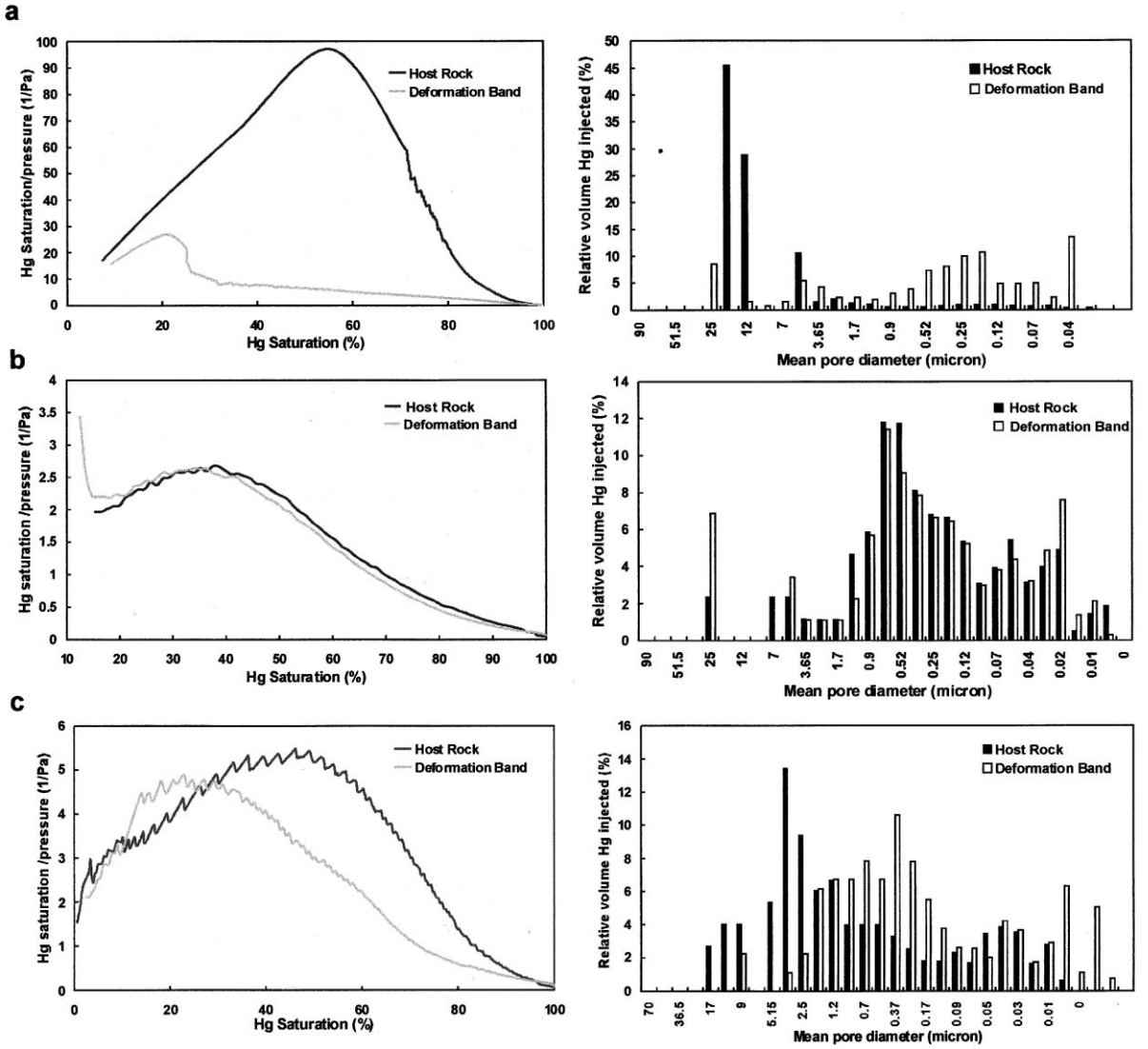

Fig. 6. Apex saturations and MICP pore size distributions for (a) cataclastic, (b) cataclastic cemented and (c) clay-rich deformation bands and host rock.

cataclastic deformation bands relative to their host (Fig. 3a). These deformation bands have a mean capillary entry pressure of 1.9×10^6 Pa compared to their host rock which requires only 4.4×10^5 Pa for initial injection of mercury. The host samples have a flatter plateau section of the capillary pressure curve compared to deformed material due to the mercury forming a well-connected thread through the sample as a result of better-sorted pore apertures. Consequently, the host rock samples have considerably lower capillary entry pressures and reach saturation more abruptly (Fig. 3; Table 1). Cemented cataclastic deformation bands sport curves, which have an almost identical morphology to their host, and these samples require much greater capillary entry pressures compared to other samples (Fig. 3b). In the clay-rich samples, a mean pressure of 1.7×10^6 Pa characterises the entry of Hg into the host rock compared to 2.9×10^6 Pa for the deformed

material (Fig. 3c). These curves may also be expressed as effective pore radii distributions. The mean pore throat radii for all deformation bands are quite similar to their host rock (Table 1). In fact, the clay-rich deformation bands have a mean value of 1.8 μm, which is greater than that of their host samples (1.3 μm). Grain size distributions for host rock and deformation bands are similar for the clay-rich samples, i.e. very poorly-sorted distributions (Fig. 4a). However, relatively well-sorted (high porosity) host sandstones grade into a bimodal cataclastic deformation band distribution (e.g. Fig. 4b). The coarse mode represents the fraction of stronger grains that have preferentially survived, survival becoming easier as grains around them become crushed, smaller and more supportive.

4.3. Irreducible water saturations

Irreducible water saturation, S_{WI}, was calculated from the MICP data to quantify the storage capacities of the deformation bands and their hosts. The cataclastic and dilational deformation bands have the greatest difference in S_{WI} relative to their host rock, i.e. up to 9× greater (Fig. 5), and hence the lowest fluid storage capacities. Clay-rich and cataclastic cemented deformation bands also have high S_{WI}, which are not significantly greater than that of their host rocks indicating low storage capacities but the ability to support large fluid columns.

4.4. Apex saturations

Apex hyperbolae calculated from MICP data are a useful way of representing the point in a pore system, which most significantly contributes to flow [34]. Apex saturations for representative deformation bands and host rock are illustrated in Fig. 6 together with MICP-derived pore size distributions.

The apex saturations for the cataclastic deformation bands and host rock indicate very different flow properties (Fig. 6a). Those of the deformation bands are considerably narrower than that of the host rock and are skewed towards lower levels of saturation (ca. 20%). This coincides with a poorly-sorted pore size distribution from 0.5 to 0.03 μm. The host rock has a well-sorted, unimodal pore size distribution from 12 to 20 μm and apex saturation at 55%.

The cemented cataclastic (Fig. 6b) deformation bands do not have significantly different apex volumes to the host rock. These have the most similar flow properties to their host rock. Pore size distributions for these samples are virtually identical, with a spread of pore sizes between 30 and 0.003 μm being indicative of poorly-sorted pores. Some samples have smaller pore sizes relative to their host, but have a similar poorly-sorted pore size distribution.

Apex distributions for clay-rich (Fig. 6c) samples show a coarse mode (macropores, >1 μm) constituting the dominant pore aperture classes and a weaker secondary mode (micropores, <1 μm) for both host and deformation band samples. The coarse mode of the deformation bands from 3.65 μm to 0.37 μm corresponds to an apex saturation of 20%, which represents the pore size range that controls fluid flow. The coarse mode of the host rock is from 15 to 0.37 μm, which coincides with a shift in the apex towards 30% saturation. These curves also testify to the very similar flow properties of clay-rich deformation bands and their host rock.

4.5. Permeability

Slip-corrected permeabilities are calculated using Hassler sleeve gas permeametry on core plugs and using pressure decay probe permeametry on the cores themselves.

The reduction in slip-corrected permeability (K_L) from host rock plugs to those containing deformation bands depends upon plug orientation, the number of deformation bands making up the sample, the amount of attached host rock in the latter, and the host rock composition. The deformation bands hosted by high porosity host rocks have the greatest difference in permeability, relative to their host. In the clay-rich cases, host rock K_L is not markedly different from plugs containing single deformation bands, and little difference is observed between deformation band permeability in a vertical or horizontal

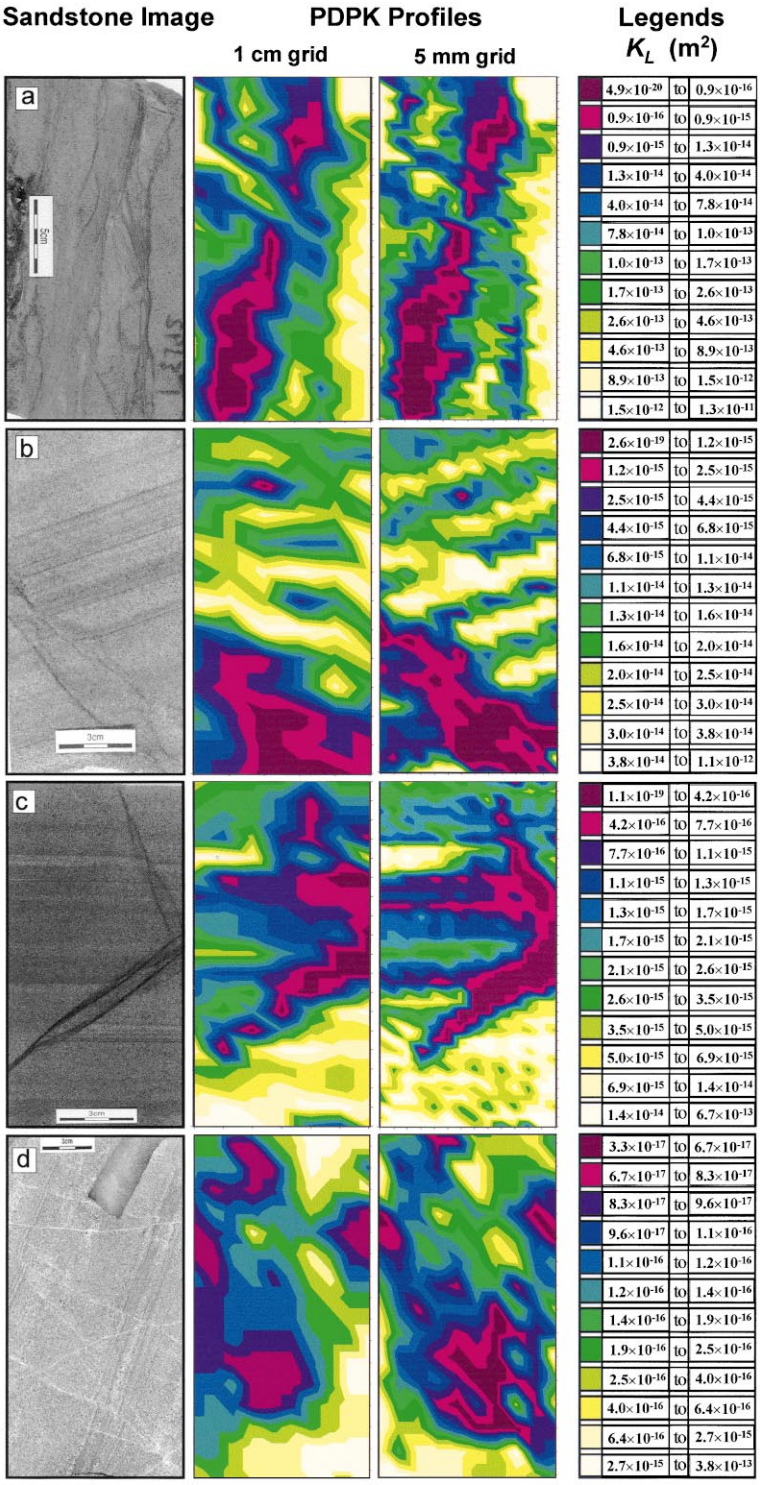
Sandstone Image
PDPK Profiles
1 cm grid
5 mm grid
Legends
K_L (m²)
a
b
c
d
4.9×10⁻²⁰ to 0.9×10⁻¹⁶
0.9×10⁻¹⁶ to 0.9×10⁻¹⁵
0.9×10⁻¹⁵ to 1.3×10⁻¹⁴
1.3×10⁻¹⁴ to 4.0×10⁻¹⁴
4.0×10⁻¹⁴ to 7.8×10⁻¹⁴
7.8×10⁻¹⁴ to 1.0×10⁻¹³
1.0×10⁻¹³ to 1.7×10⁻¹³
1.7×10⁻¹³ to 2.6×10⁻¹³
2.6×10⁻¹³ to 4.6×10⁻¹³
4.6×10⁻¹³ to 8.9×10⁻¹³
8.9×10⁻¹³ to 1.5×10⁻¹²
1.5×10⁻¹² to 1.3×10⁻¹¹
2.6×10⁻¹⁹ to 1.2×10⁻¹⁵
1.2×10⁻¹⁵ to 2.5×10⁻¹⁵
2.5×10⁻¹⁵ to 4.4×10⁻¹⁵
4.4×10⁻¹⁵ to 6.8×10⁻¹⁵
6.8×10⁻¹⁵ to 1.1×10⁻¹⁴
1.1×10⁻¹⁴ to 1.3×10⁻¹⁴
1.3×10⁻¹⁴ to 1.6×10⁻¹⁴
1.6×10⁻¹⁴ to 2.0×10⁻¹⁴
2.0×10⁻¹⁴ to 2.5×10⁻¹⁴
2.5×10⁻¹⁴ to 3.0×10⁻¹⁴
3.0×10⁻¹⁴ to 3.8×10⁻¹⁴
3.8×10⁻¹⁴ to 1.1×10⁻¹²
1.1×10⁻¹⁹ to 4.2×10⁻¹⁶
4.2×10⁻¹⁶ to 7.7×10⁻¹⁶
7.7×10⁻¹⁶ to 1.1×10⁻¹⁵
1.1×10⁻¹⁵ to 1.3×10⁻¹⁵
1.3×10⁻¹⁵ to 1.7×10⁻¹⁵
1.7×10⁻¹⁵ to 2.1×10⁻¹⁵
2.1×10⁻¹⁵ to 2.6×10⁻¹⁵
2.6×10⁻¹⁵ to 3.5×10⁻¹⁵
3.5×10⁻¹⁵ to 5.0×10⁻¹⁵
5.0×10⁻¹⁵ to 6.9×10⁻¹⁵
6.9×10⁻¹⁵ to 1.4×10⁻¹⁴
1.4×10⁻¹⁴ to 6.7×10⁻¹³
3.3×10⁻¹⁷ to 6.7×10⁻¹⁷
6.7×10⁻¹⁷ to 8.3×10⁻¹⁷
8.3×10⁻¹⁷ to 9.6×10⁻¹⁷
9.6×10⁻¹⁷ to 1.1×10⁻¹⁶
1.1×10⁻¹⁶ to 1.2×10⁻¹⁶
1.2×10⁻¹⁶ to 1.4×10⁻¹⁶
1.4×10⁻¹⁶ to 1.9×10⁻¹⁶
1.9×10⁻¹⁶ to 2.5×10⁻¹⁶
2.5×10⁻¹⁶ to 4.0×10⁻¹⁶
4.0×10⁻¹⁶ to 6.4×10⁻¹⁶
6.4×10⁻¹⁶ to 2.7×10⁻¹⁵
2.7×10⁻¹⁵ to 3.8×10⁻¹³

direction. Furthermore, bedding orientation may have a greater effect in permeability reduction than deformation band orientation, e.g. sample D9 cut normal to the host rock lamination has an order of magnitude permeability less than that of horizontal deformation band plug D9 and vertical host rock plug H9 (Table 1).

Paired *t*-tests were run on HSGP data using SigmaStat 2.03™ for clay-rich and cataclastic deformation bands and their host rocks to quantify the difference between host rock and deformation band permeabilities. For the clay-rich deformation bands $P = 0.019$ and for the cataclastic deformation bands $P = 0.03$. In both cases, $P < 0.05$ indicating a $>95\%$ probability that there is significant difference between the host rock and deformation band Hassler sleeve gas permeametry data sets.

4.6. Pressure decay probe permeametry

Pressure decay probe permeametry (PDPK) profiles demonstrate the microscale variations in permeability in small volumes of rocks within and around deformation band zones and individual strands of deformation bands. In most cases the individual strands split and recombine forming isolated host rock pods.

Pervasive zones of extensional, millimetre-thick, cataclastic bands in the highly porous sandstones are delineated as primary regions of permeability reduction (Fig. 7a). There are reductions up to four orders of magnitude compared with the permeability of the adjacent host rock, and a five order of magnitude reduction compared to the bulk host rock. The regions of most advanced grain comminution (Fig. 1a) have mean permeabilities as low as 9.8×10^{-20} m^2 (10^{-4} mD), and therefore are likely fault seals.

In the clay-rich sandstones there is a mean reduction in permeability of two orders of magnitude for the deformation bands (to 9.8×10^{-16} m^2; 1 mD) compared to the clay-rich host rock (Fig. 7b,c), and a five order of magnitude reduction in permeability occurs from the deformation bands into the intervening host rock pods. In this region the permeability drops to 1.9×10^{-19} m^2 (2×10^{-4} mD), illustrating the potential of these zones of clay-rich deformation bands as barriers to fluid flow and their excellent fault seal qualities. However, the influence of clay-rich deformation bands as barriers to fluid flow is often matched by variations in laminae thickness and variations of grain size within laminae. For example the dark laminae in Fig. 7b have a comparable permeability to the deformation bands and have up to five orders of magnitude lower permeability values relative to neighbouring lighter coloured laminae. The deformation band zones also have a large influence outside their boundaries as evidenced by regions of low permeability occurring as haloes outside the limits of the deformation band zone (Fig. 7b).

A more accurate portrayal of the micro-permeability of host rock pods and deformation bands was achieved using 5 mm grid spacing as opposed to 1 cm grid spacing. The increased grid resolution shows regions of lowest permeability coinciding with individual (1–2 mm thick) strands and laminae on the core image (Fig. 7b,c). In Fig. 7d, a 1 cm grid spacing underestimates permeability in this sample, whereas at 5 mm grid resolution swarms of anhydrite and dolomite cemented cataclastic deformation bands coincide with well-constrained regions of permeability, and reductions of up to two orders of magnitude to 1.98×10^{-17} m^2 (0.02 mD) are measured across the deformation bands. By contrast, core plug measured (K_L) permeability shows reductions up to one order of magnitude in clay-rich deforma-

←

Fig. 7. Pressure decay probe permeametry (PDPK) maps of sandstones containing deformation bands, accompanying images and legends. Note that the reliability of permeabilities lower than 10^{-18} m^2 is questionable. (a) Reductions in permeability of four orders of magnitude in pervasive, cataclastic deformation bands relative to highly porous host sandstones. (b,c) Less severe reductions in clay-rich deformation bands (mean of two orders of magnitude), hosted by low porosity clay-rich sandstones. At a 5 mm grid resolution the interplay between sedimentary and structural permeability barriers is illustrated. (d) Swarms of anhydrite and dolomite cemented deformation bands with a mean of two orders of magnitude reduction in permeability relative to the well-laminated sandstones of the host rock.

tion bands and up to two orders of magnitude for cataclastic deformation bands (Table 1). Nevertheless these measurements serve to illustrate that there is up to two orders of magnitude less permeability in plugs containing cataclastic bands oriented normal to flow compared to those parallel to flow. Plugs containing clay-rich deformation bands have similar permeabilities in a direction parallel or normal to gas flow (Table 1).

5. Conclusions

High-resolution petrophysical data generated in this study in relation to the microstructure of deformation bands enables more accurate predictions of the sealing capabilities of various deformation bands to be made. Deformation bands have throws on the millimetre-scale and hence are not resolvable using seismic mapping techniques. Therefore, prediction from the microscale, i.e. from a 'process' point of view, is a potentially powerful tool.

Pressure decay probe permeametry (PDPK) and image analysis porosimetry have been used to provide measurements on 2D volumes of individual deformation bands at finer spatial resolution than commonly used techniques. The data must be collected at the millimetre-scale (i.e. 5 mm grid spacing) as only at this resolution the permeability of individual structures and other surrounding potential flow barriers can be effectively delineated. A much smaller grid in PDPK is expected to give greater permeability heterogeneity. These measurements should be combined with more conventional techniques which sample 3D rock volumes. For example, mercury injection capillary pressure (MICP) analysis provides useful deformation band-specific, porosity, pore size distribution and S_{WI} data.

The results provide a framework for classifying common types of deformation bands in terms of their petrophysical properties. These are as follows:

- Cataclastic deformation bands result from grain size reductions, grain packing and reductions in sorting, and often contain a large amount of host-sized grains. Zones of deformation bands have PDPK permeabilities from 4.9×10^{-20} m^2 (10^{-5} mD) to 4.0×10^{-14} m^2 (40 mD) and HSGP measures of up to two orders of magnitude reduction in permeability within deformation bands. These deformation bands have porosity reductions of up to 50% relative to their host rock, however, occasionally greater reductions are recorded using thin-section image analysis. They have up to 6× greater irreducible water saturations (S_{WI}) relative to the host rock and therefore considerably lower fluid storage capacities compared with the host rock. Cataclastic deformation bands are therefore primary baffles to flow in the high porosity sandstones studied and, depending upon geometrical distribution, qualify as fault seals.

- Despite having the poorest quality fabrics (i.e. poorly-sorted and texturally immature) and therefore highest potential sealing capacities the clay-rich deformation bands have very similar petrophysical properties to their host. These have PDPK permeabilities up to two orders of magnitude less than that of their host rocks, and negligible differences in HSGP permeabilities are measured relative to their hosts. Moreover, by reducing the PDPK grid spacing from 1 cm to 5 mm, certain dark sedimentary laminae are shown also to have significant reductions in porosity and permeability, and therefore are also likely to influence fluid flow. These together with image analysis porosity measurements show a greater difference than the conventional measurements in petrophysical values between host rock and deformation band. Porosity reductions up to 25% are measured; slightly greater differences are measured using thin-section porosimetry.

- The analysis of cemented deformation bands has a large geohistory component, i.e. the amount of cementation is controlled by burial histories, fault reactivation, etc., and they are most effective in modifying the flow properties of rocks with high depositional porosity and permeability. This is the case with the fluorite

cemented dilational deformation bands where porosity is reduced by up to 75% and permeability reduced by up to five orders of magnitude. Many of the cements studied are localised in distribution within highly crushed (well-sorted) fabrics, but act to structurally tighten already low porosity and permeability fault rocks. For example, PDPK measurements map swathes of permeability from 3.3×10^{-17} m^2 (0.03 mD) to 1.1×10^{-16} m^2 (0.11 mD), which coincide with these deformation band zones. It is clear that these deformation bands may not have such a large influence upon fluid flow as first appearance in core sample suggests.

These results are by no means universally applicable, as different reservoirs have had varying geohistories (i.e. degree of consolidation, depth of burial and the stress states), and have different lithologies. Nevertheless, this study provides high-resolution porosity and permeability data together with conventional petrophysical data from common types of deformation bands, categorised in terms of their fault seal potential. The results provide valuable calibration for well log sampling of deformation bands. Moreover integration of such data with borehole imagery (e.g. FMI), seismic attribute mapping and outcrop studies of fault geometry distributions is crucial for effective fault seal analysis.

Acknowledgements

We would like to thank Conoco UK Ltd and The Carnegie Trust for the Universities of Scotland for sponsoring this work, and to Core Laboratories UK (Aberdeen) Ltd for the use of their pressure decay probe permeameter. Thanks also to Colin Taylor and John Still, University of Aberdeen, for their technical assistance.*[AC]*

References

[1] H.E. Edwards, A.D. Becker, J.A. Howell, Compartmentalisation of an aeolian sandstone by structural heterogeneities: Permo-Triassic Hopeman Sandstone, Moray Firth, Scotland, in: C.P. North, D.J. Prosser (Eds.), Characterisation of Fluvial and Aeolian Reservoirs, Geol. Soc. Spec. Publ. 73, 1993, pp. 339–365.

[2] S.J. Hippler, Deformation microstructures and diagenesis in sandstone adjacent to an extensional fault: Implications for the flow and entrapment of hydrocarbons, Bull. Am. Assoc. Petrol. Geol. 77 (1993) 625–637.

[3] M. Antonellini, A. Aydin, D.D. Pollard, Microstructure of deformation bands in porous sandstones at Arches National Park, Utah, J. Struct. Geol. 16 (1994) 941–959.

[4] M. Antonellini, A. Aydin, Effect of faulting on fluid flow in porous sandstones; petrophysical properties, Bull. Am. Assoc. Petrol. Geol. 78 (1994) 355–377.

[5] R.G. Gisbon, Physical character and fluid-flow properties of sandstone-derived fault zones, in: M.P. Coward, T.S. Daltaban, H. Johnson (Eds.), Structural Geology in Reservoir Characterization, Geol. Soc. Lond. Spec. Publ. 127, 1998, pp. 83–97.

[6] Q.J. Fisher, R.J. Knipe, Fault sealing processes in siliciclastic sediments, in: G. Jones, Q.J. Fisher, R.J. Knipe (Eds.), Faulting, Fault Sealing and Fluid Flow in Hydrocarbon Reservoirs, Geol. Soc. Lond. Spec. Publ. 147, 1998, pp. 117–135.

[7] R.J. Knipe, Q.J. Fisher, G. Jones, M.B. Clennell, A.B. Farmer, B. Kidd, E McAllister, J.R. Porter, E.A. White, Fault Seal prediction methodologies, applications and successes, in: P. Møller-Pedersen, A.G. Koestler (Eds.), Hydrocarbon Seals - Importance for Exploration and Production, NPF Spec. Publ. 7, 1997, pp. 15–38.

[8] A. Aydin, Small faults formed as deformation bands in sandstone, Pure Appl. Geophys. 116 (1978) 913–930.

[9] A. Aydin, A.M. Johnson, Analysis of faulting in porous sandstones, J. Struct. Geol. 5 (1983) 19–31.

[10] K. Mair, I. Main, S. Elphick, Sequential growth of deformation bands in the laboratory, J. Struct. Geol. 22 (2000) 25–42.

[11] R.J. Knipe, G.E. Lloyd, Microstructural analysis of faulting in quartzite, Assynt, NW Scotland: implications for fault zone evolution, Pure Appl. Geophys. 143 (1994) 229–254.

[12] E.D. Pittman, Effect of fault-related granulation on porosity and permeability of Quartz Sandstones, Simpson Group (Ordovician), Oklahoma, Bull. Am. Assoc. Petrol. Geol. 65 (1981) 2381–2387.

[13] J. Fowles, S. Burley, Textural and permeability characteristics of faulted, high porosity sandstones, Mar. Petrol. Geol. 11 (1993) 608–623.

[14] J.T. Engelder, Cataclasis and the generation of Fault Gouge, Bull. Am. Assoc. Petrol. Geol. 85 (1974) 1515–1522.

[15] G. Sammis, G. King, R. Biegel, The kinematics of gouge deformation, Pure Appl. Geophys. 125 (1987) 777–812.

[16] R.B. Berg, A.H. Avery, Sealing properties of Tertiary growth faults, Texas Gulf coast, Bull. Am. Assoc. Petrol. Geol. 79 (1995) 375–393.

[17] N.G. Lindsay, F.C Murphy, J.J. Walsh, J. Watterson, Outcrop studies of shale smears of fault surfaces, Spec. Publ. Int. Assoc. Sed. 15 (1993) 113–123.
[18] E. Sverdrup, K. Bjorlykke, Small faults in sandstones from Spitzbergen and Haltenbanken and their relation to fluid flow, in: R.M. Larsen, H. Brekke, B.T. Larsen, E. Talleraas (Eds.), Structural and Tectonic Modelling and its Application to Petroleum Geology, NPF Spec. Publ. 1, Elsevier, Amsterdam, 1992, pp. 507–517.
[19] R.G. Gibson, Fault-zone seals in siliclastic strata of the Columbus basin, Offshore Trinidad, Bull. Am. Assoc. Petrol. Geol. 78 (1994) 1372–1385.
[20] S.D. Burley, J. Mullis, A matter, timing and diagenesis in the Tartan Reservoir (UK North Sea): constraints from combined cathodoluminescence microscopy and fluid inclusion studies, Mar. Petrol. Geol. 6 (1989) 98–120.
[21] D.L. Smith, B. Evans, Diffusional crack healing in quartz, J. Geophys. Res. 89 (1984) 4125–4136.
[22] B.J. Kowallis, H.F. Wang, B.A. Jang, Healed microcrack orientations in granite from Illinois borehole UPH-3 and their relationship to the rocks stress history, Tectonophysics 135 (1987) 297–306.
[23] M. Antonellini, A. Aydin, Effect of faulting on fluid flow in porous sandstones; geometry and spatial distribution, Bull. Am. Assoc. Petrol. Geol. 79 (1995) 642–671.
[24] W.R. Jamison, D.W. Stearns, Tectonic deformation of Wingate Sandstone, Colorado National Monument, Bull. Am. Assoc. Petrol. Geol. 66 (1982) 2584–2608.
[25] R.H. Gabrielsen, R.K. Aarland, E. Alsaker, Identification and spatial distribution of fractures in porous, siliciclastic sediments, in: M.P. Coward, T.S. Daltaban, H. Johnson (Eds.), Structural Geology in Reservoir Characterization, Geol. Soc. Lond. Spec. Publ. 127, 1998, pp. 49–64.
[26] S.R. Ogilvie, J.M. Orribo, P.W.J. Glover, The influence of deformation bands upon fluid flow using profile permeametry and positron emission tomography, Geophys. Res. Lett. 28 (2000) 61–64.
[27] B.K. Atkinson, Fracture Mechanics of Rock, Academic Press, London, 1987, 534 pp.
[28] G.P. Leveille, R. Knipe, C. More, D. Ellis, G. Dudley, G. Jones, Q.J. Fisher, G. Allinson, Compartmentalisation of Rotliegendes gas reservoirs by sealing faults, Jupiter Fields area, southern North Sea, in: K. Ziegler, P. Turner, S.R. Daines (Eds.), Petroleum Geology of the Southern North Sea: Future Potential, Geol. Soc. Lond. Spec. Publ. 123, 1998, pp. 87–104.
[29] R.H. Sibson, McM. Moore, A.H. Rankin, Seismic pumping-a hydrothermal fluid transport mechanism, J. Geol. Soc. Lond. 131 (1975) 653–659.
[30] R.H. Sibson, Fluid flow accompanying faulting: field evidence and models, in: D.W. Simpson, P.G. Richards (Eds.), Earthquake Prediction: An International Review, Maurice Ewing Series 4, American Geophysical Union, 1981, pp. 593–603.
[31] I.G. Main, O.K. Kwon, B.T. Ngwenya, S.C. Elphick, Fault sealing during deformation band growth in porous sandstone, Geology 28 (2000) 1131–1134.
[32] J.W. Rudnicki, C.H. Chen, Stabilization of rapid frictional slip on a weakening fault by dilatant hardening, J. Geophys. Res. 93 (1998) 4745–4757.
[33] S.C. Jones, The Profile Permeameter; A new fast accurate Minipermeameter, Paper SPE 24757 presented at the 1992 SPE Technical Conference and Exhibition, Washington, October 4–7, 1992.
[34] E.D. Pittman, Relationship of porosity and permeability to various parameters derived from mercury injection-capillary pressure curves for sandstone, Bull. Am. Assoc. Petrol. Geol. 7 (1992) 191–198.